Simulation of shock-induced melting of Ni using molecular dynamics coupled to a two-temperature model

L. Koči,[1] E. M. Bringa,[2] D. S. Ivanov,[3] J. Hawreliak,[2] J. McNaney,[2] A. Higginbotham,[4] L. V. Zhigilei,[5] A. B. Belonoshko,[6,7] B. A. Remington,[2] and R. Ahuja[1,6]

[1]*Condensed Matter Theory, Physics Department, University of Uppsala, Box 530, SE-751 21 Uppsala, Sweden*

[2]*Lawrence Livermore National Laboratory, Livermore, California 94550, USA*

[3]*National Centre for Laser Applications, Galway, Ireland*

[4]*Department of Physics, Clarendon Laboratory, University of Oxford, Oxford OX1 3PU, United Kingdom*

[5]*Department of Materials Science and Engineering, University of Virginia, Charlottesville, Virginia 22903, USA*

[6]*Applied Material Physics, Department of Materials Science and Engineering, Royal Institute of Technology, 100 44 Stockholm, Sweden*

[7]*Condensed Matter Theory, Alba Nova University Center, Physics Department, Royal Institute of Technology, 100 44 Stockholm, Sweden*

(Received 29 December 2005; revised manuscript received 27 April 2006; published 6 July 2006)

Using nonequilibrium molecular dynamics (MD) simulations we study shock-induced melting in Ni with an embedded atom method (EAM). Dynamic melting is probed by the pair correlation function, and we find a melting lattice temperature of $T_{\mathrm{melt}}=6400\pm300$ K for a melting pressure of $P_{\mathrm{melt}}=275\pm10$ GPa. When a combined MD+TTM (two-temperature model) approach is used to include electronic heat conduction and electron-phonon coupling, P_{melt} and T_{melt} change. For a given pressure, the temperature behind the shock decreases due to electronic heat diffusion into the cold, unshocked material. This cooling of the material behind the shock slightly increases the melting pressure compared to simulations without electronic heat conduction and electron-phonon coupling. The decrease in the temperature behind the shock front is enhanced if the electron-phonon coupling is artificially made larger. We also explore the feasibility of using x-ray diffraction to detect melting.

DOI: 10.1103/PhysRevB.74.012101 PACS number(s): 62.50.+p

Although studied for centuries, melting is still enigmatic and the understanding of its mechanisms is still developing. A large number of recent papers discuss premelting due to defects,[1] melting of superheated metals,[2,3] and surface effects.[4] Shock waves have been used for decades to study the behavior of materials under extreme conditions.[5–7] Recently, a detailed microscopic picture of the atomistic evolution of shocked materials is emerging and a new generation of experiments is able to examine nonequilibrium properties from dynamic shock measurements.[8–12] Advances in diffraction analysis have dramatically increased the resolution of shock experiments, allowing the study of lattice response on a nanosecond time scale.[8,9] Detailed knowledge of shock-induced melting transitions will be required to accurately predict performance at the National Ignition Facility (NIF). Molecular dynamics (MD) simulations have been successfully employed to study "equilibrium" solid-liquid transitions,[13–16] including *ab-initio* simulations.[17,18] These simulations, however, do not give any information on how the material can reach the final state, or if there will be any plasticity or phase transition involved. Nonequilibrium atomistic simulations (NEMD) do provide this kind of information,[19–22] and have become a powerful tool to study shock propagation in liquids and solids. Characteristic times in strong shock experiments can be achieved by MD, making possible a direct comparison between simulations and experiments.[20,21]

There have been studies of shock-induced melting using NEMD in Ar,[19] where interactions are well described by pair potentials. Recent simulations have also addressed the shock melting of Cu[20] and Fe.[22] The goal of the present investigation is to focus on MD simulations of shock-induced melting of Ni, using an embedded-atom model (EAM) potential. MD simulations only include "lattice heat conduction." Electronic heat conduction and electron-phonon coupling can be incorporated, however, using a two-temperature model (TTM),[23] calculating the lattice temperature and the electron temperature separately. Although the TTM is an approximate way to treat electronic effects, it has been successfully used to model laser material interactions in mixed MD+TTM approaches.[23,24] In this paper, we are interested in how the electronic effects could reduce the temperature behind the shock due to electronic heat conduction and preheating of the material in front of the shock. These effects could lead to changes in the shock strength required to melt the solid, as compared to calculations without electronic effects.

Shock simulations were carried out as described elsewhere,[21,25] using an EAM Ni potential.[26] This potential gives a single crystal Hugoniot that deviates from existing experimental values for polycrystalline Ni, as shown in Fig. 1, since it was not fit to high-pressure data. We use this potential only as an example of what would occur with a typical EAM fcc metal. In addition, "real" materials contain large concentrations of defects such as impurities and grain boundaries. These defects could change the shock melting temperature, as measured experimentally. For the sake of simplicity, the role of these defects will be neglected in this study. The temperature dependent parameters of the electronic TTM equation and properties of the EAM Ni material are given in Refs. 23, 24, and 27. We have used a 3D solver

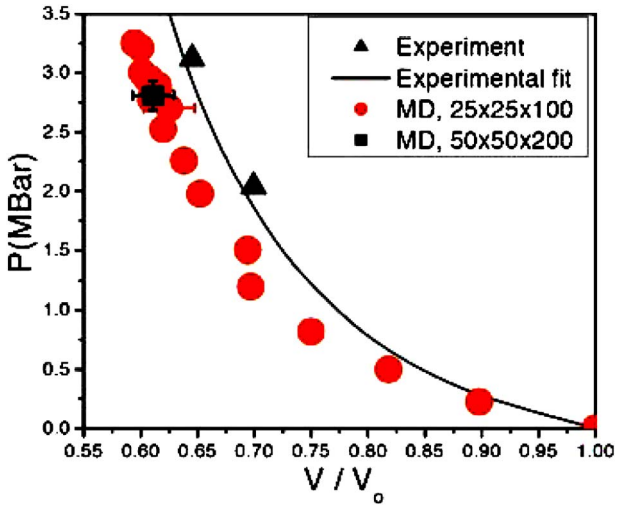

FIG. 1. (Color online) Equation of state for single crystal Ni samples. The MD numbers indicate the size of the system in fcc unit cells (Ref. 25). Experiments for polycrystalline Ni are also shown (two representative data points and a fit from Ref. 32).

for the heat diffusion equation, with cubic cells of side ~0.5 nm.[27] The electron-phonon coupling G is a function of density and temperature, but using constant values of G has proved sufficient to fit experimental data. Since we are mainly interested in a model calculation, we also choose a value of $G=G_0$ that is constant. In order to test the influence of G on melting, we have used both the generally accepted G_0 value and also changed this value by a factor of 10, leaving everything else the same.

Figure 2(a) shows a snapshot of our sample for a shock strength well below the melting threshold. Crystallinity is maintained, but dislocations are emitted behind the shock front, as shown for both pair and many-body potentials.[20] Figure 2(b) shows a snapshot of the sample for a shock strength above the melting threshold. The pair correlation function $g(r)$ for several pressures at a time when the shock front is near to the back side of our sample is shown in Fig. 3. All atoms in front of the shock front, as well as a few layers directly behind the shock front were neglected. Atoms up to a few layers in front of the piston were also neglected. The decrease of the peaks beyond first nearest neighbor marks the onset of melting. The $g(r)$ curves in the range 275–295 GPa practically overlap. Experimentally, the structure and long-range order can be studied with x-ray diffraction[29] and be related to the results of MD simulations,[30] as shown in Fig. 4. The characteristic signs of melting are shown by the increase in the peak width and drop in intensity. This could be measured with time resolved Bragg diffraction.[8] The three dimensional structure of the reciprocal lattice spot, which gives information about the dislocation structure in the material, could be measured using diffuse scattering techniques.

The data for the electronic temperature profiles at different times for $P=320$ GPa is presented in Fig. 5. The lattice temperature behind the shock goes down, and the lattice temperature immediately ahead of the shock increases, which is due to fast electronic heat conduction and electron-phonon

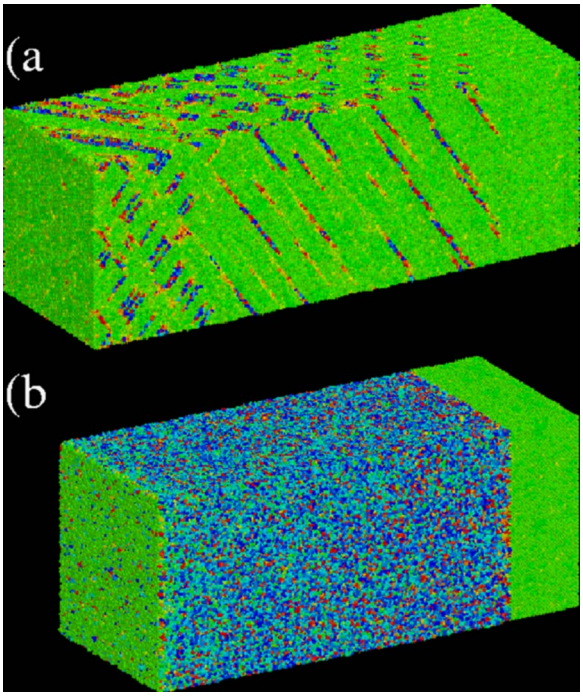

FIG. 2. (Color online) Snapshots of MD simulations. The shock wave moves from left to right. The coloring uses the centrosymmetry parameter (Ref. 28). (a) $P=50$ GPa, showing dislocation loops and (b) $P=280$ GPa, showing disorder (melt) behind the front.

coupling. The variation of the electronic temperature in the plane perpendicular to the shock front was small (~5%). This is in contrast to large localized variations in the lattice temperature, of up to 40%. After 2.5 ps, the electronic temperature had not yet reached equilibrium with the lattice temperature. This could lead to preheating of the lattice and the generation of a thermal wave.[31] The melting pressure as determined from our simulations could also change, and this change could be estimated from TTM simulations embedded in continuum codes, which can handle much larger spatial and temporal scales.

Figure 6 shows the lattice temperature behind the shock

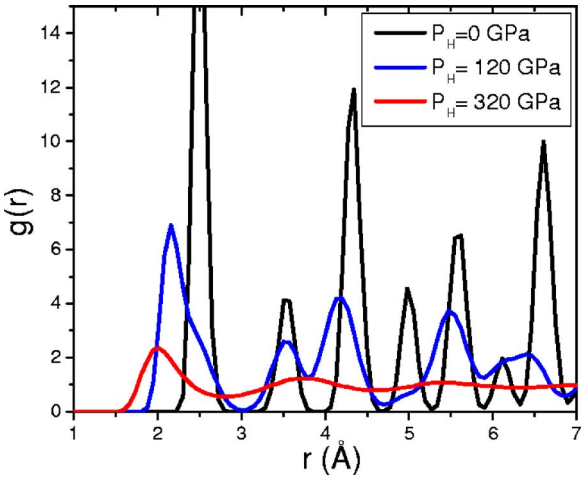

FIG. 3. (Color online) Pair correlation function $g(r)$ for several shock pressures.

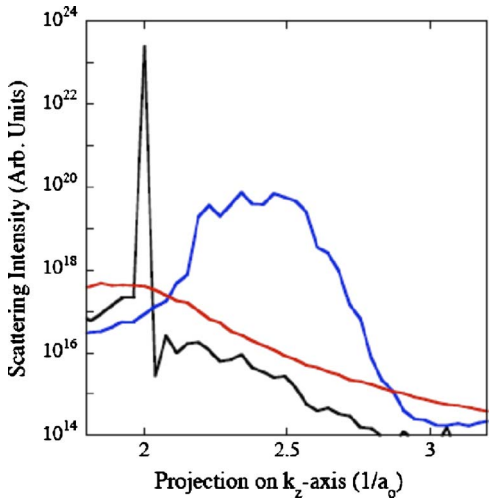

FIG. 4. (Color online) Simulated x-ray diffraction of MD snapshots, with a 3D Fourier transform. Unshocked sample (black); heavily dislocated sample at $P=50$ GPa (blue); structure just above melting at $P=280$ GPa (red). The projection on the z axis, which corresponds to the Bragg diffraction of (00l) planes, shows a shift to a higher wave number, indicating lattice compression, and significant broadening and reduction in intensity (blue curve) as the material approaches melt. Once past the threshold for melt, the signal loses all structure (red).

front at different pressures. There is no clear kink in the diagram that would indicate a phase transition. From the $g(r)$ (Fig. 3), we obtain a melting pressure, P_{melt}, of 275 ± 10 GPa, 285 ± 10 GPa, and 290 ± 10 GPa, for MD, MD+TTM, and MD+TTM$\times10$, respectively. This was confirmed by the visual inspection of snapshots, colored to show crystalline regions and defects (Fig. 2). As expected, the melting pressure increases, as the lattice temperature decreases due to electronic heat conduction, and increases if the electron-phonon coupling is artificially increased. However, the pressure shift is of the order of our estimated uncertainty, and comparable to typical experimental errors of a few percent. The experimental dataset for shocked Ni near the melt transition is very scarce,[32–34] but a Lindemann-type model[33,34] gives a shock-melting pressure of ~330 GPa. However, numerous high-pressure experiments indicate the inadequacy of the Lindemann criterion to estimate the pressure dependence of the melting temperature.[35] The liquid-solid coexistence simulations predict a lower melting temperature than the MD and the MD+TTM at the same pressure. Although superheating in shock simulations should be small due to dislocations, recent results indicate a maximum bulk superheating of over 20%.[36] Thus, the higher melting temperatures for the MD and the MD+TTM compared to the coexistence simulations shown in Fig. 6 are reasonable.

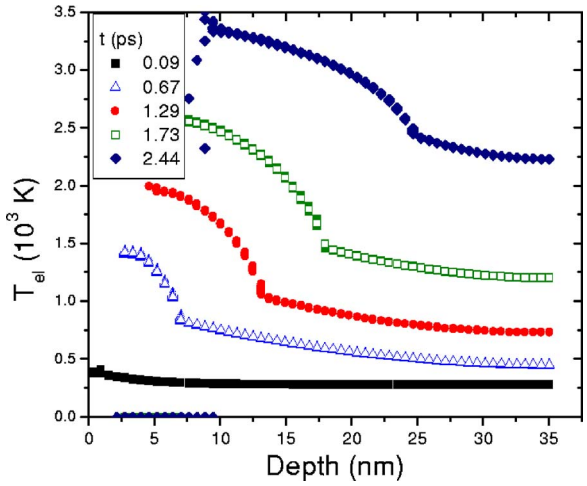

FIG. 5. (Color online) Electronic temperature profiles at different times, for $P=320$ GPa. The hump coincides with the location of the shock wave and the rise of the lattice temperature.

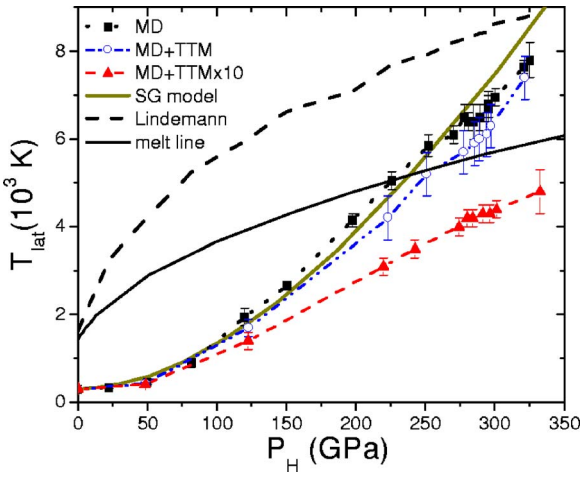

FIG. 6. (Color online) Pressure-temperature diagram for MD (black), MD+TTM (blue), and MD+TTM$\times10$ (red). Error bars for the pressure are less than 5% of its value. Also shown: melt line from liquid-solid coexistence simulations with the EAM potential; shock temperature from the Steinberg-Guinan (SG) model (Refs. 33 and 34); and a Lindemann melt line (using the density from MD at each pressure as reference) predicting a shock-melt pressure ~10% higher that our MD simulations.

As the melting pressure increase for the MD+TTM is approximately 10 GPa (15 GPa for the MD+TTM$\times10$) compared to the MD without TTM, our simulations show that the inclusion of electronic effects leads to a relatively small increase in the melting pressure.

The preheating leads to a temperature change ahead of the shock front, which is small compared to the heating behind the shock front. Thus, its effects on melting are small for the time scale of our simulations, being just a few ps. However, the effect could be significant for longer pulses, materials with larger electron-phonon coupling, or if the temperature increase is enough to cause a phase change.

Experiments using ultra short intense laser pulses may be able to detect differences between equilibrium melting and "nonequilibrium" melting. For equilibrium melting, the electronic temperature is the same as the lattice temperature, whereas for "nonequilibrium" melting, the lattice can disorder while the electronic system remains relatively cold. In addition, better knowledge of shock-melt temperatures is needed for NIF ignition experiments: to optimize performance, the first shock in a staged-shock drive needs to be at the minimum pressure necessary to melt the capsule ablator.[37]

The authors would like to thank B. Sadigh, G. Gilmer, B. Torralva, and A. Caro for fruitful discussions and P. Erhart for help analyzing simulation results. The work at LLNL was performed under the auspices of the U.S. Department of Energy and Lawrence Livermore National Laboratory under Contract No. W-7405-Eng-48. We are also grateful to VR, Sweden, for financial support.

[1] A. M. Alsayed, M. F. Islam, J. Zhang, P. J. Collings, and A. G. Yodh, Science **309**, 1207 (2005).
[2] F. Forsblom and G. Grimvall, Nat. Mater. **4**, 388 (2005).
[3] S.-N. Luo, T. J. Ahrens, T. Çağin, A. Strachan, W. A. Goddard III, and D. C. Swift, Phys. Rev. B **68**, 134206 (2003).
[4] B. J. Siwick, J. R. Dwyer, R. E. Jordan, and R. J. Dwayne Miller, Science **302**, 1382 (2003).
[5] W. J. Nellis, J. A. Moriarty, A. C. Mitchell, M. Ross, R. G. Dandrea, N. W. Ashcroft, N. C. Holmes, and G. R. Gathers, Phys. Rev. Lett. **60**, 1414 (1988).
[6] A. C. Mitchell, W. J. Nellis, J. A. Moriarty, R. A. Heinle, N. C. Holmes, R. E. Tipton, and G. W. Repp, J. Appl. Phys. **69**, 2981 (1991).
[7] W. J. Nellis, A. C. Mitchell, and D. A. Young, J. Appl. Phys. **93**, 304 (2003).
[8] A. Loveridge-Smith, A. Allen, J. Belak, T. Boehly, A. Hauer, B. Holian, D. Kalantar, G. Kyrala, R. W. Lee, P. Lomdahl, M. A. Meyers, D. Paisley, S. Pollaine, B. Remington, D. C. Swift, S. Weber, and J. S. Wark, Phys. Rev. Lett. **86**, 2349 (2000).
[9] M. A. Meyers, F. Gregori, B. K. Kad, M. S. Schneider, D. H. Kalantar, B. A. Remington, G. Ravichandran, T. Boehly, and J. S. Wark, Acta Mater. **51**, 1211 (2003).
[10] P. Celliers, A. Ng, G. Xu, and A. Forsman, Phys. Rev. Lett. **68**, 2305 (1992).
[11] T. Löwer, V. N. Kondrashov, M. Basko, A. Kendl, J. Meyer-ter-Vehn, R. Sigel, and A. Ng, Phys. Rev. Lett. **80**, 4000 (1998).
[12] A. Ng and T. Ao, Phys. Rev. Lett. **91**, 035002 (2003).
[13] J. Q. Broughton and X. P. Li, Phys. Rev. B **35**, 9120 (1987).
[14] J. Mei and J. W. Davenport, Phys. Rev. B **46**, 21 (1992).
[15] C. Dai, H. Tan, and H. Geng, J. Appl. Phys. **92**, 5019 (2002).
[16] B. Sadigh, M. Dzugutov, and S. R. Elliott, Phys. Rev. B **59**, 1 (1999).
[17] S. A. Bonev, B. Militzer, and G. Galli, Phys. Rev. B **69**, 014101 (2004).
[18] M. P. Surh, T. W. Barbee III, and L. H. Yang, Phys. Rev. Lett. **86**, 5958 (2001).
[19] A. B. Belonoshko, Science **275**, 995 (1997).
[20] E. M. Bringa, J. U. Cazamias, P. Erhart, J. Stölken, N. Tanushev, B. D. Wirth, R. E. Rudd, and M. J. Caturla, J. Appl. Phys. **96**, 3793 (2004).
[21] E. M. Bringa, A. Caro, Y. Wang, M. Victoria, J. M. McNamey, B. A. Remington, R. F. Smith, B. R. Torralva, and H. Van Swygenhoven, Science **309**, 1838 (2005).
[22] K. Kadau, T. C. Germann, P. S. Lomdahl, and B. L. Holian, Phys. Rev. B **72**, 064120 (2005).
[23] D. S. Ivanov and L. V. Zhigilei, Phys. Rev. B **68**, 064114 (2003).
[24] L. V. Zhigilei and D. S. Ivanov, Appl. Surf. Sci. **248**, 433 (2005).
[25] Samples ($25\times25\times100$ to $50\times50\times200$ fcc cells) were prismatic with free surfaces along the shock direction [001] and periodic boundary conditions (PBC) in the directions transverse to the shock wave. They were equilibrated at 300 K before a "piston" was moved at the desired piston velocity, U_p, leading to a shock front with velocity U_s. The pressure behind the shock was calculated from the Hugoniot equations as $P_H=\rho_0 U_s U_p$, with the initial density ρ_o.
[26] X. W. Zhou, H. N. G. Wadley, R. A. Johnson, D. J. Larson, N. Tabat, A. Cerezo, A. K. Petford-Long, G. D. W. Smith, P. H. Clifton, R. L. Martens, and T. F. Kelly, Acta Mater. **49**, 4005 (2001).
[27] L. V. Zhigilei, D. S. Ivanov, E. Leveugle, B. Sadigh, and E. M. Bringa, Proc. SPIE **5448**, 505 (2004).
[28] C. L. Kelchner, S. J. Plimpton, and J. C. Hamilton, Phys. Rev. B **58**, 11085 (1998).
[29] K. Rosolankova *et al.*, *Shock Compression of Condensed Matter—2003*, edited by M. D. Furnish, Y. M. Gupta, and J. W. Forbes (APS, New York, 2004), pp. 1195–1198.
[30] Z. Lin and L. V. Zhigilei, unpublished.
[31] V. F. Nesterenko, A. M. Staver, and B. K. Styron, Combust., Explos. Shock Waves **9**, 378 (1975).
[32] Shock wave data, http://www.ficp.ac.ru/rusbank/
[33] D. J. Steinberg, "Equation of state and strength properties of selected materials," Lawrence Livermore National Laboratory Report, UCRL-MA-106439, 1991; D. J. Steinberg, J. Appl. Phys. **51**, 1498 (1980).
[34] M. A. Meyers, *Dynamic Behavior of Materials* (Wiley, New York, 1994).
[35] L. H. Cohen, W. Klement, and G. C. Kennedy, Phys. Rev. **145**, 519 (1966).
[36] A. B. Belonoshko, N. V. Skorodumova, A. Rosengren, and B. Johansson, Phys. Rev. B **73**, 012201 (2006).
[37] T. R. Dittrich, S. W. Haan, M. M. Marinak, S. M. Pollaine, D. E. Hinkel, C. P. Verdon, G. L. Strobel, R. McEachern, R. C. Cook, C. C. D. C. Wilson, P. A. Bradley, L. R. Foreman, and W. S. Varnum, Phys. Plasmas **6**, 2164 (1999).